

Observing Interfacial Sliding Processes in Solid–Solid Contacts

Kathryn J. Wahl and W. Gregory Sawyer

Abstract

Directly seeing into a moving contact is a powerful approach to understanding how solid lubricants develop low-friction, long-lived interfaces. In this article, we present optical microscopy and spectroscopy approaches that can be integrated with friction monitoring instrumentation to provide real-time, *in situ* evaluation of solid lubrication phenomena. Importantly, these tools allow direct correlation of common tribological events (such as variations in friction and wear) with the responsible sliding-induced mechanical and chemical phenomena. We demonstrate the utility of *in situ* approaches with applications to a variety of thin-film solid lubricants.

Introduction

Interfacial films generated from solid–solid contacts are ubiquitous in everyday life, ranging from visible scuffing of floors by dark shoe soles and tire skid marks on pavement to transfer of graphite, wax, or chalk to surfaces during writing. Many engineering systems, too, depend on selective formation of solid interfacial films to reduce friction and wear during startup. Operation of spacecraft components such as antennas, bearings, bushings, restraints, and latches depends on successful solid-phase lubrication under exposure to extreme thermal and environmental conditions. Airfoil bearings currently under development for gas turbine engines require lubrication during startup and spin-down before sufficient aerodynamic lift is generated to separate surfaces; similar issues are encountered in the computer hard disk and read–write head interface. Because the interfaces controlling friction and wear processes are “buried” inside the contacts, the development of materials engineering strategies to solve lubrication problems and prevent lubricant- or wear-related failures has typically proceeded through Edisonian trial-and-error approaches. The difficulty of observing and understanding

what is happening within the sliding solid–solid interfaces has limited both the modeling of contact processes and predictive engineering to improve the performance of sliding components.

Solid lubrication of an interface requires both low, stable friction and development of low-wear conditions. A common strategy for solid lubrication is surface modification with a lubricant-containing coating. Unfortunately, because coatings are typically worn away during operation, their lifetimes are limited. This has motivated alternative strategies to resupply lubricants during operation (e.g., delivery of solid lubricant powders¹ or *in situ* formation of solid lubricants from the gas phase^{2–7}).

Because sliding occurs in a buried interface, it is challenging to determine what materials processes are actively enabling stable performance. Similarly, unknown interfacial phenomena cause friction instabilities and debris generation to occur, and wear can go undetected. This article highlights recent advances of *in situ* tribology instrumentation and approaches that allow observation and quantification of the mechanical and chemical processes influencing friction and wear in solid-

lubricated contacts. These new approaches allow for an understanding of issues such as: What causes friction instabilities? How do chemistry and mechanics combine to provide low friction? How does varying the ambient environment change the interfacial film morphology and rheology? How do crystal structure and size influence lubricant performance?

Several benefits can be obtained by performing tribological measurements *in situ* in the test environment. First, it simplifies the correlation between friction data and interface events. Second, it eliminates the need to remove the sample from the test environment and thus greatly reduces the risk of surface contamination. Perhaps most importantly, much of the highly speculative nature of deriving explanations for friction changes can be eliminated from direct observation of contact events in real time.

Instrumentation

In its simplest form, a tribometer is a device that measures friction forces. (Normal forces might or might not be directly measured, and many designs exist that apply a normal load through a “deadweight.”) However, to move beyond a simple measurement of friction and try to understand the physical processes and transformations occurring within the sliding interface, one needs to devise methods to monitor more than these forces. There is a rich history of tribologists examining contacts with varied *in situ* approaches, including contact resistance, conductance, thermoelectric, interferometric, and thermal measurements.⁸ *In situ* approaches continue to be useful in tribology. Recent examples include interrogating the contact at higher spatial resolution either from within the tribometer itself (by measuring electrical contact resistance^{9–12} or temperature¹³) or building a tribometer that allows another instrument to monitor the contact in real time.^{14–21}

To perform microscopy or spectroscopy within a sliding contact, the test geometry and materials must allow measurements through at least one of the interfaces perpendicular to the plane of contact, or parallel to the sliding interface. For optical observations or visible light spectroscopy, one or both of the sliding surfaces must be transparent. Early use of transparent contacts with interferometry to quantify thickness changes in contacts was pioneered by Tabor and colleagues^{22–24} using crossed mica cylinders. The surface-force apparatus (SFA) geometry has been applied to studies of liquid-film sliding contacts (see, for example, McGuiggan et al.²⁵), with the

ability to examine subtle molecular motions in confinement.^{26,27} Including Raman spectroscopy with SFA techniques can add chemical specificity^{21,28} and x-ray diffraction through thin interfaces is also possible.²⁰ However, the delicate nature of the interface, typically mica sheets, makes studying solid lubrication phenomena with SFA difficult. Macroscopic, direct observations of interfacial film motion,^{19,29–31} thickness changes,^{32–35} and wear,^{12,36,37} as well as chemistry using Raman microscopy^{19,34,38,39} and Fourier transform infrared (FTIR) spectroscopy,¹⁷ have been demonstrated for solid-lubricated contacts. Chemical probes, such as Raman spectroscopy might require additional considerations, such as excitation wavelength to reduce fluorescence backgrounds or selectively induce resonance enhancements to the signal. An alternative possibility, observation through the side of the contact, is difficult because the interfacial films formed from solid–solid sliding contacts are typically very thin (<1 μm). Instrumentation advances in transmission electron microscopy (TEM) have enabled visualization of small, electron-transparent contacts directly in real time (see the article by Marks et al. in this issue). Alternatively, the contact can be “frozen” in place by focused-ion-beam (FIB) sectioning techniques and examined by high-resolution TEM.⁴⁰

In Situ Chemical and Microstructural Transformation during Sliding

It is well-established that thin, deformable solid films can lower friction between two hard surfaces by forming an easily sheared layer to accommodate sliding.^{8,40,41} Solid lubricants, such as dichalcogenides (MoS₂, WS₂, WSe₂), graphite, and diamondlike carbon (DLC), and soft metals, such as silver and indium, can all reduce friction by forming interfacial, or transfer, films at the sliding interface. How such coatings lower friction is less clear; possibilities include development of a slip interface between the interfacial film and substrate, deformation of the interfacial film, or even more complex motions catalogued by Godet and Berthier.^{42–44} Chemical reactions and mechanical transformation (often referred to as tribochemical and tribomechanical processes, respectively) can also take place: amorphous materials can crystallize, crystalline materials can reorient or be amorphized, and surfaces can oxidize or form other reaction products under sliding stresses. Ultimately, to understand how solid lubricants work, it is important to determine what material is actually lubricating the

interface and how it is accomplishing that task.

One method to examine interfacial sliding processes is by combining visual observation through a transparent, stationary counterface with micro-Raman spectroscopy for chemical analysis (Figure 1); this geometry is used in the test instrument at the U.S. Naval Research Laboratory (NRL).^{19,30–35,37–39} Experimentally, it would be more convenient to observe the contact through the flat substrate rather than through a curved hemisphere used to generate high stresses and facilitate alignment. However, most solid lubricants, which are typically applied to the flat substrate, are not optically transparent at visible wavelengths. Solid lubricants prepared by modern physical and chemical vapor deposition approaches are thus better studied through the uncoated contact. This approach will work as long as the interfacial films remain relatively thin. If the interfacial films become substantially thicker than the optical mean free path of the film itself at the observing wavelength (typically 500–800 nm), the optical microscopy or Raman signal can miss measuring the interface and instead probe only the back side of the interfacial film. Fortunately, a wide array of solid lubricant phenomena can be examined without significant interference from these potential problems.

An illustrative example of how *in situ* tribometry can assist in explaining solid lubrication phenomena is sapphire sliding against a boric acid film on a hard B₄C substrate. Boric acid readily forms from boron oxide in the presence of water vapor (B₂O₃ + 3H₂O → 2H₃BO₃) and is a good solid lubricant.^{45–47} By heat treating a B₄C engineering surface in an oxidizing environment, a boron oxide-containing surface layer can be formed.⁴⁸ When a counterface is rubbed against an oxidized B₄C substrate in humid air, the resulting boric acid surface layer provides low-friction sliding. Eventually, the boron oxide layer is worn away, and the friction increases when boric acid is no longer available to lubricate the contact. *In situ* Raman tribometry experiments confirmed that this lubrication mechanism does occur: Boric acid was observed in the sliding interface when friction was low, and when the Raman signal for boric acid disappeared, the friction increased.¹⁹ These experiments also revealed a second lubricating phase: carbon. This surface carbon was an additional reaction product formed during oxidation of B₄C at 800°C, where B₄C reacts with O₂ to produce B₂O₃, C, and gaseous products CO and CO₂. *In situ* Raman tribometry initially detected

both boric acid and carbon bands in the contact; the friction coefficient was slightly higher than for lubrication by boric acid alone (μ ≈ 0.08 vs. μ ≈ 0.06). When the boric acid signal disappeared, the carbon signal remained, and the friction coefficient increased to μ ≈ 0.2. These experiments demonstrated that boric acid was the primary lubricating phase and that the friction was almost as low as that for boric acid alone. However, once boric acid was depleted from the contact, carbon took over as the material in the interface with the lowest friction.

In situ techniques also have been used to monitor structural changes in materials such as crystallization of MoS₂. In one example, a glass counterface was slid against a metal-doped MoS_x coating (Pb–Mo–S) having initially featureless x-ray diffraction and Raman spectra.³¹ These and similar coatings are scientifically interesting in that doping disrupts the growth of crystalline MoS₂ and often produces improved wear resistance without sacrificing friction performance. *In situ* micro-Raman spectroscopy identified the formation of crystalline MoS₂ in the interface within 66 sliding cycles³¹ after low-friction sliding was obtained; this is consistent with *ex situ* Raman studies of Pb–Mo–S and similar materials^{49–51} that revealed crystalline MoS₂ both on the worn coating and in the interfacial transfer film on the stationary counterface. Although this experiment did not verify exactly *where* the crystalline transformation occurred (that is, in the transfer film or at the coating surface), later cross-sectional high-resolution TEM experiments demonstrated a monolayer of crystalline MoS₂ on the coating surface oriented parallel to the sliding surface⁵¹ and hints of new layers forming below the surface. The experiments confirmed that the low friction of nominally amorphous Pb–Mo–S coatings was due to transformation to ordered crystalline MoS₂ and sliding of crystalline MoS₂ against crystalline MoS₂.

Recently, Hu and co-workers⁵² built a microtribometer inside a scanning electron microscope (SEM) equipped with a FIB and sample lift-out apparatus. The key advantage of the instrument involves the ability to fabricate a TEM specimen from a “stopped” sliding contact (Figure 2). To do this, a sliding test is run for the desired number of cycles using a sacrificial silicon carbide tip sliding against the surface of interest. The test is then stopped, and FIB milling is commenced at the sacrificial microscale tungsten tip. Redeposition of sputtered material covers and protects the sliding interface from damage, and several specimens contain-

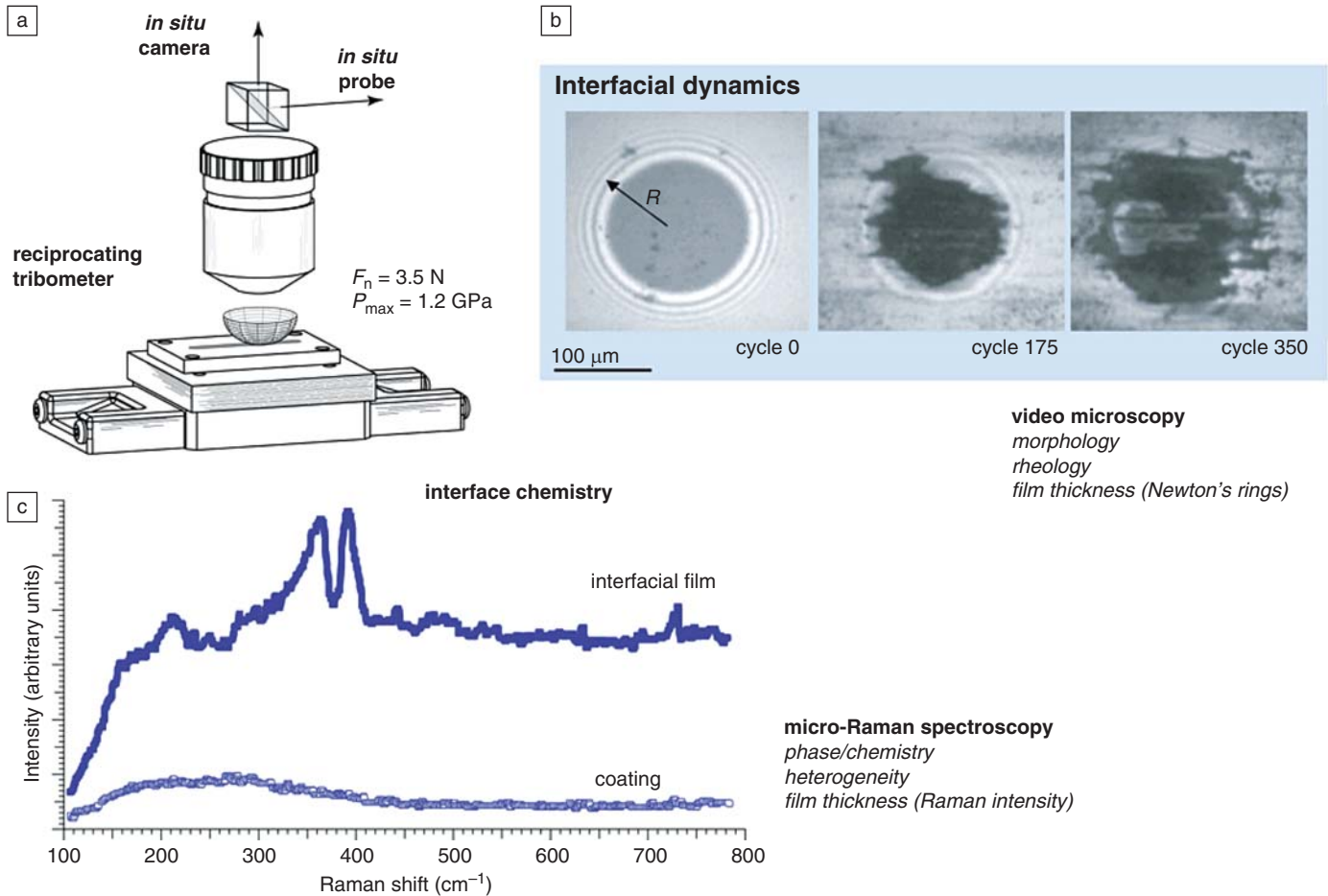


Figure 1. (a) Illustration of the test configuration for *in situ* video microscopy and Raman spectroscopy through a transparent hemisphere. (b) Examples of interfacial film formation. The first image shows the contact and associated interference fringes before sliding takes place. The middle image shows that a stationary (as observed in real time) interfacial film has formed at the interface, and the image on the right shows the interfacial film thinning and shearing in the center of the contact. (c) Unworn Pb–Mo–S solid lubricant coating showing featureless Raman spectrum compared to the spectrum after sliding showing that sliding has transformed the interfacial film to MoS_2 .

ing the tip/wear track surface with an intact sliding interface can be obtained. The first experiments using this apparatus demonstrated that sliding contact against crystalline WSe_2 coatings transformed the surface microstructure, with both reorientation and recrystallization of the WSe_2 layers observed (Figure 2, upper right). The technique holds much promise for detailed investigation of the mechanical and chemical changes occurring in sliding contacts that had previously been accessible only through *ex situ* TEM methods.^{53,54}

Interfacial Film Formation

The previous examples of lamellar lubrication with dichalcogenides such as MoS_2 and WSe_2 raise the question of where and how low-friction sliding is taking place. Although many have proposed a “deck-of-cards” analogy for sliding of

layered lubricants, it is not yet clear how many (or how few) layers are needed to accommodate interfacial shear with low friction. Are one or more layers needed on both counterbodies? It is known that transferred crystallites are often found aligned parallel to the sliding interface.⁵⁵ Some evidence suggests that sliding a MoS_2 -containing transfer film against a recrystallized track might be all that is required.^{51,56} The recent work by Hu and co-workers⁵² leaves the question open: Some noncontacting regions of the frozen interface have no transfer film, whereas both the contacting and gap regions have similar numbers of transformed layers. New materials such as fullerene-like MoS_2 and WS_2 particles are also of great interest, as they too can provide very low-friction sliding. Is the lubrication mechanism the same as for lamellar dichalcogenide coatings? Some have speculated that rolling

might occur in a mechanism akin to nanoscale ball bearings, although evidence for particle flattening and exfoliation under stress suggests otherwise.^{57,58} Real-time, *in situ* TEM experiments hold the genuine possibility of answering the fundamental question of how lamellar solid lubricants actually accommodate motion during sliding.

Although an atomic-scale understanding of interfacial slip in macroscopic and microscale solid-lubricated contacts is not yet a reality, monitoring solid lubrication processes with optical techniques has provided much insight into how materials such as MoS_2 and DLC provide, and maintain, low friction. For example, in low-humidity environments, where MoS_2 and related materials perform best, *in situ* optical observations directly show that the velocity is accommodated by interfacial sliding. Specifically, this means that the

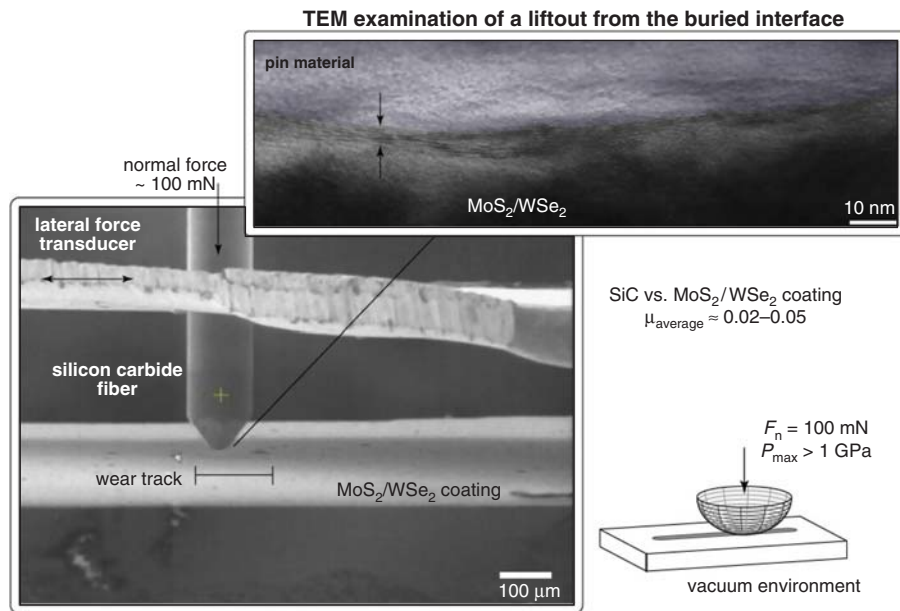


Figure 2. The *in situ* tribometer (bottom right) uses a silicon carbide fiber in sliding contact with a test specimen inside a scanning electron microscope equipped with a focused ion beam and manipulator. (Adapted in part from Reference 40.) After the sliding experiment, the contact was frozen in place (lower left) by redeposition during focused-ion-beam milling, and a sample suitable for examination by transmission electron microscopy was prepared and removed from the contact. This is shown at the upper right, where thin, aligned interfacial films are clearly visible within the contact (between arrows).

sliding occurs between a motionless interfacial film that has formed and attached to the stationary counterface and the solid lubricant coating.

Interfacial transfer-film formation and thickness can be directly monitored by optical techniques such as interferometry. Color interferometric techniques have been employed to monitor nanometer-scale thickness changes in liquid-lubricated contacts (see the article in this issue by Cann)^{16,59,60} and molecular lubrication studies using a surface-force apparatus (SFA).^{20,25,61–63} For solid-lubricated contacts, the opacity of the interfacial film to the incident light can limit the ability to quantify the interfacial film thickness. MoS₂, for example, has limited transparency at visible wavelengths.⁶⁴ However, interference fringes outside the contact, familiarly referred to as Newton's rings (Figure 3), can be used to monitor changes in the interfacial film thickness.³⁵ As the thickness of the interfacial film increases (or decreases), the interference fringes move inward (or outward). With white-light illumination, fringe separation is equivalent to a change in height of one-half of the wavelength of light, or ~270 nm. Although the ability to resolve thickness changes is limited by camera charge-coupled device (CCD) resolution and fringe sharpness, the

primary limitation is tribological, specifically, ejected debris from the sliding contact that ultimately obscures the rings. However, before this happens, much can be learned about the rate of transfer-film buildup and depletion during sliding (Figure 3, lower right), the relationship to changes in friction coefficient, and friction instabilities.^{34,35} In Ti-doped MoS₂ coatings,^{65,66} changes from low- to high-friction states are associated with the accumulation of a MoS₂ transfer film on the counterface (low friction) and then gradual removal of the interfacial film and redeposition onto the track surface, where the roughened wear track increases friction through plowing processes.

If the optical transparency of the transfer film is of the same order as its thickness, such as for DLC, it is possible to use Raman spectroscopy to quantify the interfacial film thickness *in situ*. DLC coatings are typically a mix of *sp*²- and *sp*³-bonded carbon, with strong bands in the 1300–1600 cm⁻¹ region from visible-wavelength Raman spectroscopy.⁶⁷ Films formed during sliding have enhanced signals in the D- (disordered-) and G- (graphitic-) band regions, implying increased graphite-like character, thus allowing differentiation between the coating and interfacial film chemistry (Figure 4, upper right). Scharf

and Singer^{32,33,39} used the intensity of Raman peaks from the DLC transfer film to monitor and quantify interfacial film thickness. They evaluated the Raman signal intensity at a given wavelength normal to the surface, through the interfacial film using the relationship based on Beer's law

$$I(t, \nu) = I_{\infty}^{\text{coating}}(\nu)e^{-2t/\lambda_{\text{film}}} + I_{\infty}^{\text{film}}(\nu)(1 - e^{-2t/\lambda_{\text{film}}}) \quad (1)$$

where t is the interfacial film thickness; ν is the excitation frequency; $I_{\infty}^{\text{coating}}$ and I_{∞}^{film} are the saturated Raman intensities for an infinitely thick coating and the interfacial film, respectively; and λ_{film} is the optical mean free path of the transfer film at the excitation frequency.³² Equation 1 is valid in the limit of coating thicknesses greater than the optical mean free path at the excitation frequency.³² In the experiments, the optical mean free path of visible Raman scattering (derived from 514-nm excitation) was found to be between 250 and 500 nm for the interfacial transfer films formed from sliding against (Si + O)-doped DLC. Using thickness values from *ex situ* profilometry, the Raman signal from the interfacial film (Figure 4, lower left) can be converted to thickness. Examples of *in situ* Raman spectra obtained while the contact was thinning (cycles 1,418–1,691) are shown in the central plot of Figure 4. Thinning of the transfer film to <25 nm was found to correlate with sudden increases in friction in the contact (cycles 1,600–2,000). The buildup and subsequent removal of the transfer film were consistently correlated with friction instabilities both optically and by Raman spectroscopy. In this contact, the transfer film that formed from DLC did not adhere well to the sapphire counterface and frequently fell off, exposing the sapphire. Friction coefficients were higher when sapphire was in direct contact with the DLC coating, until a transfer layer from the DLC coating again built up on the sapphire ball.

Rheology

Nearly all of the low-friction solid-lubricated sliding interfaces examined by *in situ* tribometry at NRL have shown what appears by optical microscopy to be purely interfacial sliding. For MoS₂-based lubricants such as Pb–Mo–S coatings, *in situ* Raman microscopy and other *ex situ* studies confirm that the sliding interface is crystalline MoS₂ against crystalline MoS₂.^{50,51} Interfacial sliding, coupled with no observable motion within the interfacial transfer film, implies that the mechanical strength of the interfacial film is greater than the applied shear stress.

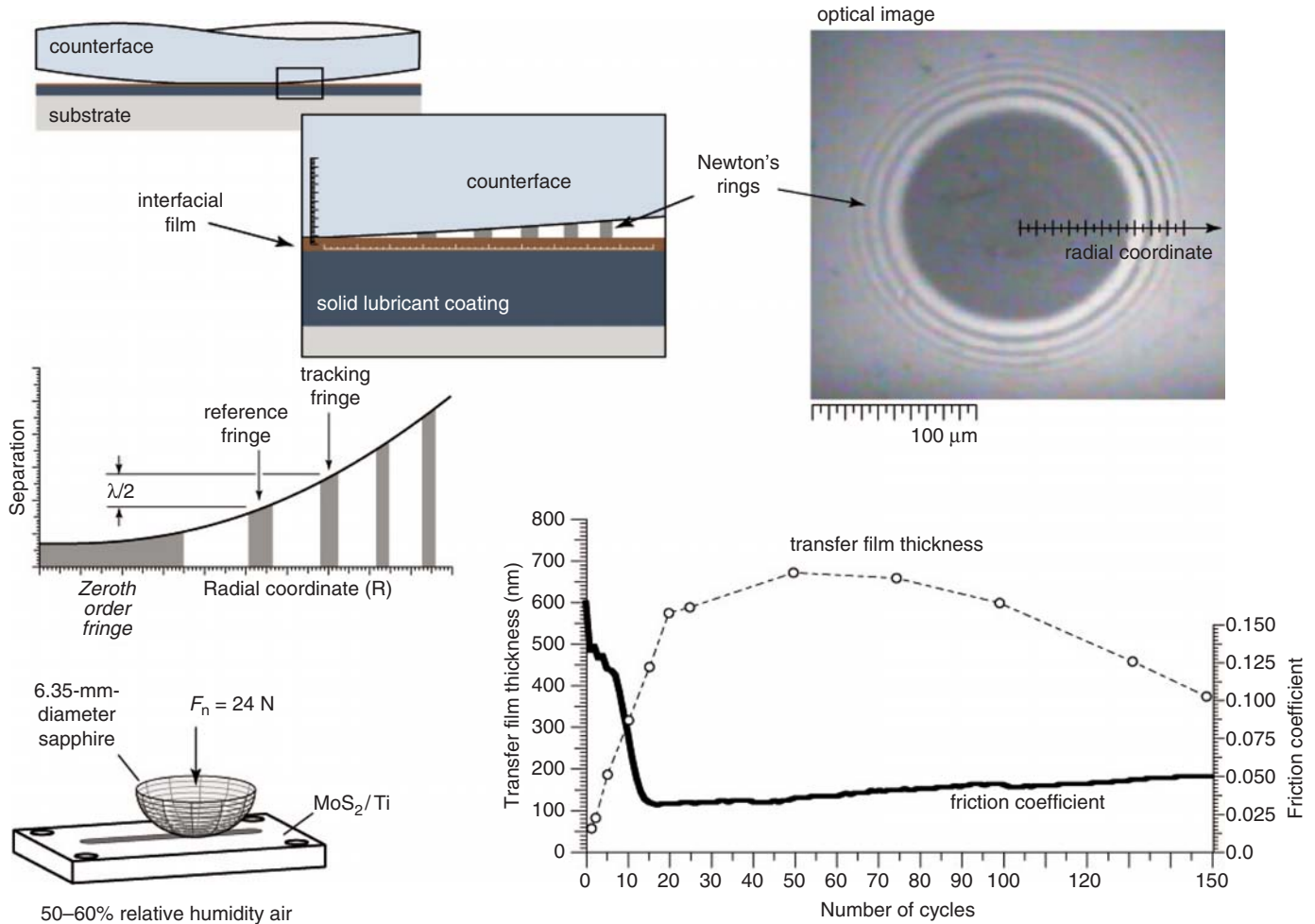


Figure 3. Thickness changes of solid lubricant interfacial films can be quantified by tracking the motions of the Newton's rings interference fringes (upper right) along a radial coordinate. Thickening of the film shifts the fringes inward, whereas thinning shifts the fringes outward. Fringes are spaced at one-half of the wavelength of the incident light (middle left), allowing nanometer-scale thickness changes to be resolved. Because the fringes are outside the contact, changes in refractive index inside the contact from formation of the interfacial film do not influence the measurement. Friction decreases as the interfacial film forms and thickens and then begins to increase slowly as the interfacial film thins and is redeposited on the track (lower right). (Adapted in part from Reference 32.)

Sliding in humid environments resulted in a sudden increase in friction coefficient and, after a short time, motion within the interfacial film.³¹ Importantly, the motion within the interfacial film was minimal and reversible as the contact reciprocated; this motion can account for only a small fraction of the sliding accommodation (<5%) based on estimates of the interfacial film thickness and measurements of the shearing distance and speed. For Pb–Mo–S coatings, motion within the transfer film in humid sliding contacts did not occur immediately upon the introduction of humidity and the accompanying increase in friction, but instead began a number of cycles later. It is likely that water penetrated the compacted interfacial film and that new, hydrated material

was added to the contact. Weakening of the interfacial film's mechanical properties in the presence of high applied shear stresses in humid environments accounted for the initiation of motion within the film. The increased friction and higher applied shear stresses in humid environments were thus implicated in causing the deformation of the interfacial film, rather than its formation, causing friction to increase. *In situ* tribology has, in this way, answered one of the questions of cause and effect in tribology: Do the interfacial films deform from high friction, or does interfacial film deformation increase friction? The former appears to be the case for this coating.

Generally, solid lubricating coatings perform well in one particular environ-

ment (e.g., dry nitrogen or vacuum at room temperature) but experience increased wear and friction when that environment is modified by the presence of oxygen, humidity, or elevated temperature. The development of nanostructured multifunctional coatings^{68–72} has resulted in improved tribological performance of solid-lubricant-containing coatings by the addition of hard phases such as carbides and nitrides. The most complex of these materials contain several solid lubricating phases such as MoS_2 or WS_2 , DLC, and Ag with the aim of providing low-friction performance in dry, humid, and high-temperature environments, respectively, as well as hard phases such as yttria-stabilized zirconia (YSZ) to improve mechanical properties.^{73,74} Many

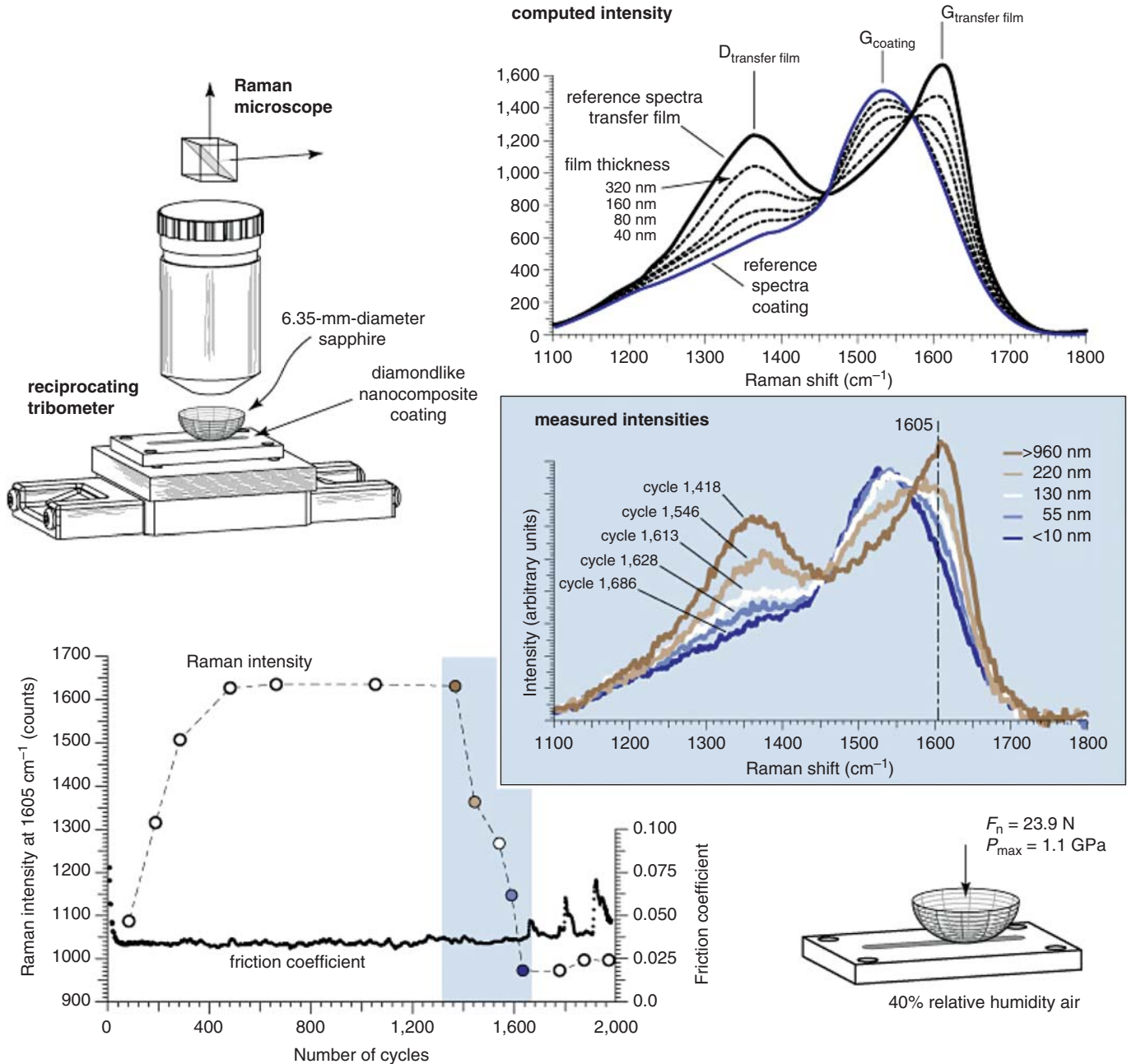


Figure 4. Quantification of thickness changes of interfacial films with Raman spectra that are distinct from those of the lubricant coating is possible when the interfacial films are sufficiently transparent. For diamondlike carbon (DLC) tribology, the interfacial transfer film formed (black reference spectrum) is spectroscopically distinct from the DLC coating (blue reference spectrum, upper right), and intensity variations between 100% interfacial film and 100% coating spectra can be computed. *In situ* spectra (blue shaded background, middle right) corresponding to the friction data displayed at the lower left of the figure clearly show these transitions. The brown spectrum shows purely interfacial film chemistry when the interfacial film exceeds the maximum quantifiable thickness (960 nm in this example), and as the interfacial film thins, a gradual transition occurs to the dark blue spectrum, where the film was <10 nm thick. This decrease in interfacial film thickness and ultimate loss of the transfer film resulted in the friction instabilities shown between 1,700 and 2,000 cycles (lower left). (Adapted, in part, from Reference 52, with permission.)

of these nanocomposites clearly showed improved friction performance during cycling from low to high humidity and at elevated temperatures,⁷⁵ as well as improved wear resistance.^{34,76} One would intuitively predict that cycling between

these environments would quickly modify the lubricating phase. Interestingly, *in situ* and *ex situ* Raman studies of the interfacial lubricating phases present in dry and humid environments for $\text{MoS}_2/\text{C}/\text{Au}/\text{YSZ}$ nanocomposites sug-

gest that the primary lubricant providing low friction at room temperature is MoS_2 .³⁴ The experiments suggest that a key mechanism to improve the mechanical performance of MoS_2 -based solid lubricants might be to provide a hard

matrix to support the MoS₂, which is then able to lubricate effectively in both dry and humid environments. *In situ* studies employing TEM approaches would enable definitive explanation of the lubrication mechanism.

Wear Monitoring

Doping MoS₂ coatings with various metals (e.g., Au, Pb, Ti) during deposition is known to disrupt the growth morphology of MoS₂.^{49,50,65,77–81} The primary benefit is derived in mitigating edge-oriented

growth conditions (with the lamellar structure's *c* axis parallel to the substrate) to increase coating density in radio-frequency-sputtered materials. For dense, basal-oriented growth morphologies, the typical result is an x-ray-amorphous coating that readily crystallizes at the sliding interface into MoS₂ lamellae^{51,56} and resists the rapid wear associated with crystalline MoS₂.⁸² Interferometry is required to monitor these materials with very low wear rates (with changes in coating thickness as low as 1 nm every 1,000 cycles⁵⁰). Although

these low wear rates can be evaluated *ex situ* with interferometry by performing multiple tests to varying sliding distances,^{50,51,82} this process is labor-intensive and precludes following wear of a particular sliding contact from start to finish.

A relatively new methodology is to build a reciprocating tribometer with an integrated scanning white-light interferometer aligned with the wear track that develops during reciprocation (Figure 5). In one embodiment of this design, both the normal and friction forces are simultaneously

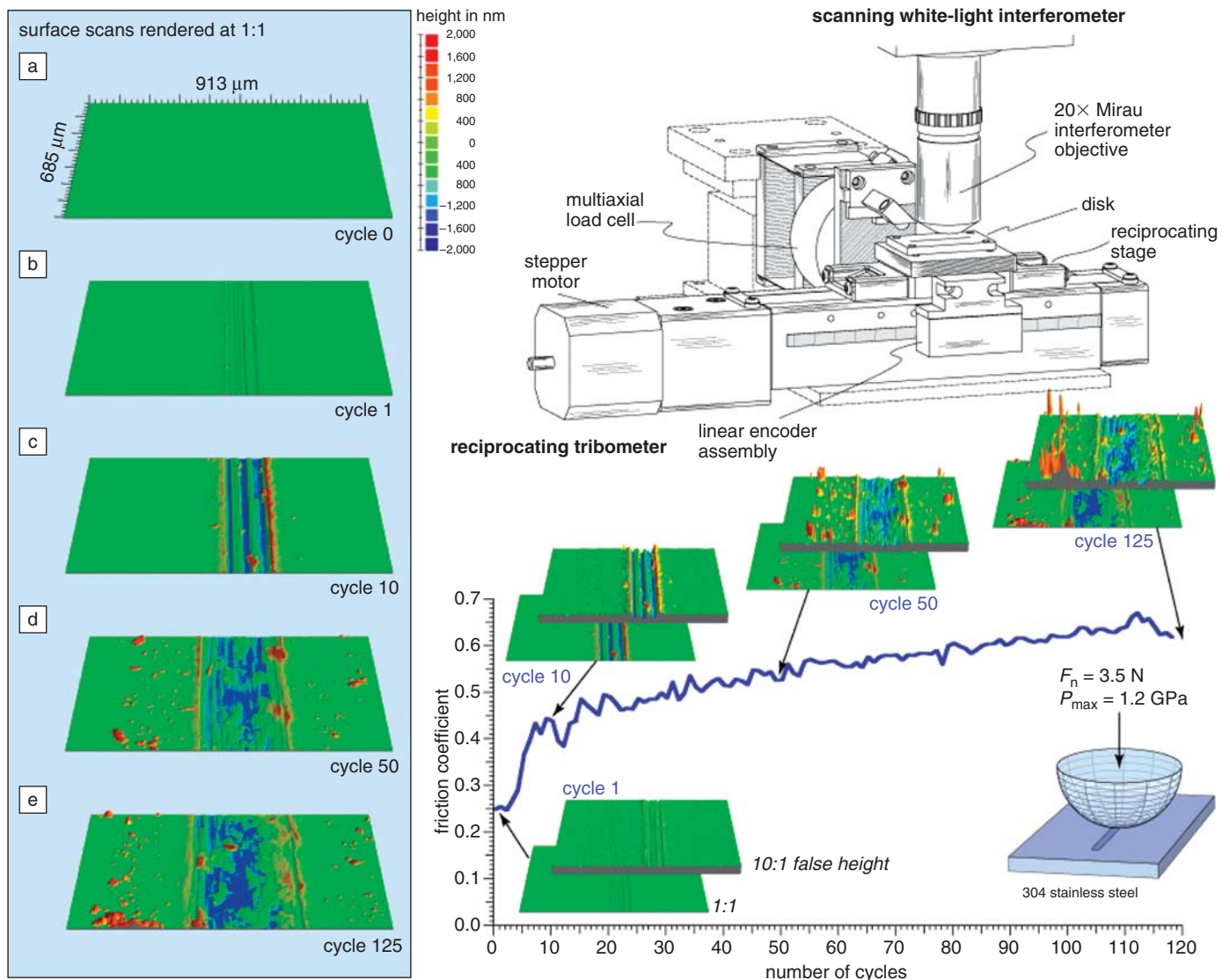


Figure 5. Wear evolution of a stainless steel wear track measured by scanning white-light interferometry. Images are rendered with perspective at a 1:1 scale, and the total range of the color map is 2 μm , although the debris (red) has typical heights of 5 μm . During the experiment, a measurement at this track position was made after every cycle. The tribometer, shown with the interferometer in the line drawing at the right, is housed within an environmental chamber and uses optical encoders and stepper motors for fine positioning under the interferometer objective after each pass. The graph at the bottom right shows the monotonic increase in friction coefficient (y axis) with number of cycles (x axis). The surface scans (a–e) are shown both in 1:1 rendering (left) and with a false height magnification of 10:1 at their respective locations in the graph at the lower right. The jump in friction coefficient around cycle 5 corresponded to deeper scratches (blue) and the first evidence of debris (red particles visible in cycles 10, 50, and 125). The gradual friction rise corresponded to a gradual increase in the width of the wear track.

measured using a multi-axis load cell and collected synchronously in a spatially resolved packet.³⁶ This allows the correlation of topographical changes at specific locations of the wear track with changes in friction and normal forces. A typical testing procedure begins by mounting the pin and counterface samples, sealing the environmental chamber, and establishing the desired environmental conditions. The counterface is then moved under the interferometer objective, and an initial surface scan is taken of the region in which the wear track will develop. A prescribed normal load is then applied between the pin and counterface, and a single (or multiple) reciprocation is then performed as the spatially resolved force data are acquired. Following reciprocation, the normal load is removed, and the surface is moved back under the interferometer objective for investigation of wear evolution. The cycle of reciprocation and interferometry is then repeated, enabling cycle-by-cycle correlations between friction and wear events. This approach allows the wear progression of a single wear track to be followed directly, rather than relying on the averaging of measurements from many tracks.

Measuring the evolution in the wear track surfaces has enabled the observation of the wear processes that take place during both initial transients and steady-state motion. As shown in Figure 5, the abrupt change in friction coefficient from $\mu = 0.25$ to $\mu = 0.45$ occurred when deep scratches first appeared on the sample, followed by debris particles that were found to move throughout the contact and its perimeter.³⁶ The friction coefficient continued to increase and was correlated with a broadening of the wear track. The deepest wear scar was around cycle 10, as debris was gradually folded back into the wear track. The wear track was found to widen through a process of discrete scratching events that left visible troughs on the edges of the contact. The wear of the unlubricated stainless steel example was dramatic in comparison with experiments on solid lubricating films similar to those shown in Figures 2 and 3. The MoS₂/WSe₂ samples had total wear depths on the order of tens of nanometers after 100 cycles, with nearly all of the wear occurring in the first 10 cycles. One can infer from the other *in situ* studies described earlier in this article that wear was likely related to formation of an interfacial film in a manner similar to that shown in Figure 3. Development of tools that simultaneously monitor both interfacial film formation and wear processes would provide a more complete picture of solid lubrication phenomena.

On the other hand, it is possible to qualitatively monitor wear of conducting coatings such as MoS₂, by contact resistance methods. In the “triboscopy” approach developed by Belin and co-workers,^{10–12} both friction and contact resistance, R_c , are monitored along the track at equally spaced intervals for each cycle. The resulting data are presented in an image format, with pixel intensity or color corresponding to friction coefficient or R_c in a manner similar to an atomic force microscopy image. This approach allows the experimenter to both clearly resolve any friction or R_c changes along the track during any given sliding cycle and follow friction or R_c changes at any given position on the track as sliding progresses. Triboscopic imaging of MoS₂ coatings enabled identification of localized damage such as pinholes in the coating and uneven wear across the track.¹² A limitation of this approach is the inability to directly monitor the morphological and thickness changes in the interfacial films. Large changes in contact resistance presumably occur when the interfacial film thickens, oxidizes, or breaks up, as is clearly observed by optical microscopy through transparent interfaces.^{19,31,34,39} Conductive transparent coatings such as indium tin oxide could enable simultaneous observation of the contact and measurement of contact resistance.

Concluding Remarks

We have highlighted the advantages of multitechnique *in situ* approaches to understanding the physical and chemical changes that enable effective solid lubrication. The difficulties of investigating hard-to-access, semitransparent materials can be overcome by applying combinations of simple optical interferometric and spectroscopic methods directly to sliding contacts. *In situ* probes have demonstrated that much of the chemical and mechanical activity in low-friction lubricating interfaces occurs over nanometer-scale vertical dimensions. Advancing the fundamental understanding of how interfacial films provide low friction will require *in situ* approaches with improved chemical, mechanical, and structural specificity, as well as increased spatial resolution.

Acknowledgments

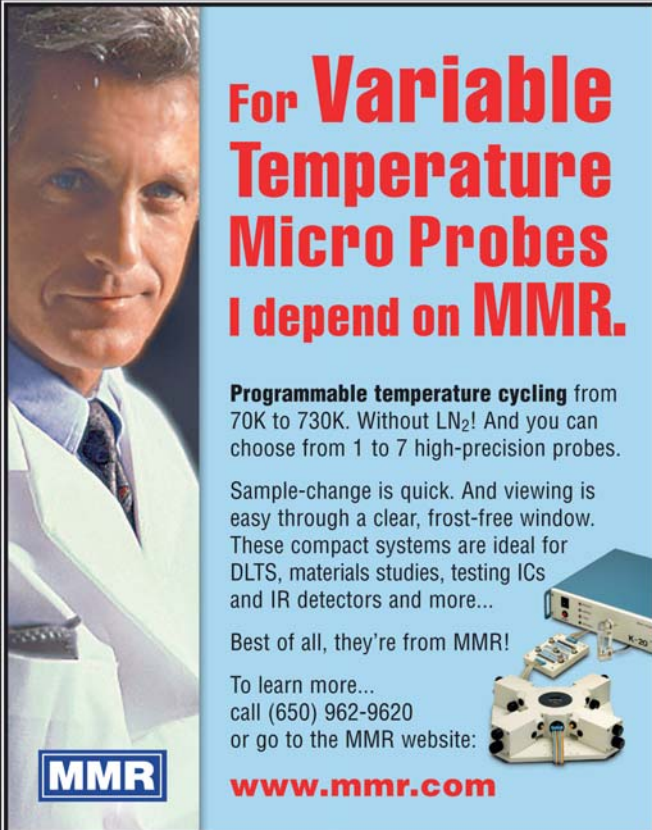
Financial support from the Office of Naval Research and the Air Force Office of Scientific Research is gratefully acknowledged.

References

1. H. Heshmat, *Tribol. Trans.* **34**, 433 (1991).
2. F.P. Bowden, J.H. Greenwood, M. Imai, *Proc. R. Soc. London, Ser. A* **304**, 157 (1968).

3. T.A. Blanchet, J.L. Lauer, Y.F. Liew, S.J. Rhee, W.G. Sawyer, *Surf. Coat. Technol.* **68**, 446 (1994).
4. I.L. Singer, T. LeMogne, C. Donnet, J.M. Martin, *Tribol. Trans.* **39**, 950 (1996).
5. I.L. Singer, T. LeMogne, C. Donnet, J.M. Martin, *J. Vac. Sci. Technol. A* **14**, 38 (1996).
6. W.G. Sawyer, T.A. Blanchet, *Wear* **229**, 581 (1999).
7. W.G. Sawyer, T.A. Blanchet, *J. Tribol.* **123**, 572 (2001).
8. F.P. Bowden, D. Tabor, *The Friction and Lubrication of Solids* (Clarendon Press, Oxford, UK, 1964), part 2.
9. L.J. Bredell, L.B. Johnson, D. Kuhlmannwilsdorf, *Wear* **120**, 161 (1987).
10. M. Belin, J.M. Martin, *Wear* **156**, 151 (1992).
11. M. Belin, J. Lopez, J.M. Martin, *Surf. Coat. Technol.* **70**, 27 (1994).
12. K.J. Wahl, M. Belin, I.L. Singer, *Wear* **214**, 212 (1998).
13. F.E. Kennedy, *Wear* **100**, 453 (1984).
14. R. Gohar, A. Cameron, *ASLE Trans.* **10**, 215 (1967).
15. J.M. Martin, M. Belin, *Thin Solid Films* **236**, 173 (1993).
16. P.M. Cann, H.A. Spikes, J. Hutchinson, *Tribol. Trans.* **39**, 915 (1996).
17. J.E. Olsen, T.E. Fischer, B. Gallois, *Wear* **200**, 233 (1996).
18. C.U.A. Cheong, P.C. Stair, *Tribol. Lett.* **10**, 117 (2001).
19. S.D. Dvorak, K.J. Wahl, I.L. Singer, *Tribol. Trans.* **45**, 354 (2002).
20. D. Gourdon, M. Yasa, A.R.G. Alig, Y.L. Li, C.R. Safinya, J.N. Israelachvili, *Adv. Funct. Mater.* **14**, 238 (2004).
21. S.C. Bae, H. Lee, Z.Q. Lin, S. Granick, *Langmuir* **21**, 5685 (2005).
22. D. Tabor, R.H.S. Winterton, *Proc. R. Soc. London, Ser. A* **312**, 435 (1969).
23. J.N. Israelachvili, D. Tabor, *Proc. R. Soc. London, Ser. A* **331**, 19 (1972).
24. J.N. Israelachvili, D. Tabor, *Wear* **24**, 386 (1973).
25. P.M. McGuiggan, M.L. Gee, H. Yoshizawa, S.J. Hirz, J.N. Israelachvili, *Macromolecules* **40**, 2126 (2007).
26. A. Mukhopadhyay, J. Zhao, S.C. Bae, S. Granick, *Rev. Sci. Instrum.* **74**, 3067 (2003).
27. F. Mugele, T. Becker, A. Klingner, M. Salmeron, *Colloid Surf. A: Physicochem. Eng. Aspects* **206**, 105 (2002).
28. S.C. Bae, J.S. Wong, M. Kim, S. Jiang, L. Hong, S. Granick, *Philos. Trans. R. Soc. A* **366**, 1443 (2008).
29. H.E. Sliney, *ASLE Trans.* **21**, 109 (1977).
30. I.L. Singer, S.D. Dvorak, K.J. Wahl, T.W. Scharf, *J. Vac. Sci. Technol. A* **21**, S232 (2003).
31. S.D. Dvorak, K.J. Wahl, I.L. Singer, *Tribol. Lett.* **28**, 263 (2007).
32. T.W. Scharf, I.L. Singer, *Tribol. Lett.* **14**, 137 (2003).
33. T.W. Scharf, I.L. Singer, *Thin Solid Films* **440**, 138 (2003).
34. R.R. Chromik, C.C. Baker, A.A. Voevodin, K.J. Wahl, *Wear* **262**, 1239 (2007).
35. K.J. Wahl, R.R. Chromik, G.Y. Lee, *Wear* **264**, 731 (2008).
36. N. Mauntler, A. Rennie, T. Schmitz, W.G. Sawyer, in *Proc. of ASPE Annual Meeting* (American Society for Precision Engineering, Monterey, CA, 2006).

37. R.R. Chromik, A.L. Winfrey, J. Luning, R.J. Nemanich, K.J. Wahl, *Wear* **265**, 477 (2008).
38. T.W. Scharf, I.L. Singer, *Tribol. Trans.* **45**, 363 (2002).
39. T.W. Scharf, I.L. Singer, *Tribol. Lett.* **14**, 3 (2003).
40. I.L. Singer, *NATO ASI Ser., Ser. E* **220**, 237 (1992).
41. I.L. Singer, *MRS Bull.* **23**, 37 (1998).
42. M. Godet, *Wear* **100**, 437 (1984).
43. Y. Berthier, M. Godet, M. Brendle, *Tribol. Trans.* **32**, 490 (1989).
44. M. Godet, *Wear* **136**, 29 (1990).
45. A. Erdemir, *Lubr. Eng.* **47**, 168 (1991).
46. A. Erdemir, G.R. Fenske, R.A. Erck, F.A. Nichols, D.E. Busch, *Lubr. Eng.* **47**, 179 (1991).
47. W.G. Sawyer, J.C. Ziegert, T.L. Schmitz, A. Barton, *Tribol. Trans.* **49**, 284 (2006).
48. A. Erdemir, C. Bindal, G.R. Fenske, *Appl. Phys. Lett.* **68**, 1637 (1996).
49. N.T. McDevitt, M.S. Donley, J.S. Zabinski, *Wear* **166**, 65 (1993).
50. K.J. Wahl, L.E. Seitzman, R.N. Bolster, I.L. Singer, *Surf. Coat. Technol.* **73**, 152 (1995).
51. K.J. Wahl, D.N. Dunn, I.L. Singer, *Wear* **230**, 175 (1999).
52. J.J. Hu, R. Wheeler, J.S. Zabinski, P.A. Shade, A. Shiveley, A.A. Voevodin, *Tribol. Lett.* **32**, 49 (2008).
53. J. Moser, F. Lévy, *Thin Solid Films* **228**, 257 (1993).
54. J.L. Grosseau-Poussard, H. Garem, P. Moine, *Surf. Coat. Technol.* **78**, 19 (1996).
55. J.M. Martin, C. Donnet, T. Lemogne, T. Epicier, *Phys. Rev. B: Condens. Matter* **48**, 10583 (1993).
56. D.N. Dunn, K.J. Wahl, I.L. Singer, "Nanostructural Aspects of Wear Behavior in Ion-Beam Deposited Pb-Mo-S Films," in *Fundamentals of Nanoindentation and Nanotribology*, N. R. Moody, W. W. Gerberich, S. P. Baker, N. Burnham, Eds., **522** (Materials Research Society, Warrendale, PA, 1998) pp. 451-456.
57. L. Cizaire, B. Vacher, T. Le Mogne, J.M. Martin, L. Rapoport, A. Margolin, R. Tenne, *Surf. Coat. Technol.* **160**, 282 (2002).
58. L. Joly-Pottuz, J.M. Martin, F. Dassenoy, M. Belin, G. Montagnac, B. Reynard, N. Fleischer, *J. Appl. Phys.* **99**, 023524 (2006).
59. R.P. Glovnea, A.K. Forrest, A.V. Olver, H.A. Spikes, *Tribol. Lett.* **15**, 217 (2003).
60. P.M. Cann, H.A. Spikes, *Tribol. Lett.* **19**, 289 (2005).
61. M.L. Gee, P.M. McGuigan, J.N. Israelachvili, A.M. Homola, *J. Chem. Phys.* **93**, 1895 (1990).
62. M. Heuberger, M. Zach, N.D. Spencer, *Science* **292**, 905 (2001).
63. R. Tadmor, N.H. Chen, J.N. Israelachvili, *J. Colloid Interface Sci.* **264**, 548 (2003).
64. B.L. Evans, P.A. Young, *Proc. R. Soc. London, Ser. A* **284**, 402 (1965).
65. D.G. Teer, J. Hampshire, V. Fox, V. Bellido-Gonzalez, *Surf. Coat. Technol.* **94-95**, 572 (1997).
66. N.M. Renevier, V.C. Fox, D.G. Teer, J. Hampshire, *Surf. Coat. Technol.* **127**, 24 (2000).
67. J. Robertson, *Adv. Phys.* **35**, 317 (1986).
68. A.A. Voevodin, J.P. O'Neill, J.S. Zabinski, *Surf. Coat. Technol.* **119**, 36 (1999).
69. R. Hauert, J. Patscheider, *Adv. Eng. Mat.* **2**, 247 (2000).
70. A.A. Voevodin, J.S. Zabinski, *Thin Solid Films* **370**, 223 (2000).
71. T. Zehnder, P. Schwaller, F. Munnik, S. Mikhailov, J. Patscheider, *J. Appl. Phys.* **95**, 4327 (2004).
72. J. Patscheider, *MRS Bull.* **28**, 180 (2003).
73. A.A. Voevodin, J.J. Hu, T.A. Fitz, J.S. Zabinski, *Surf. Coat. Technol.* **146**, 351 (2001).
74. A.A. Voevodin, T.A. Fitz, J.J. Hu, J.S. Zabinski, *J. Vac. Sci. Technol. A* **20**, 1434 (2002).
75. C.C. Baker, R.R. Chromik, K.J. Wahl, J.J. Hu, A.A. Voevodin, *Thin Solid Films* **515**, 6737 (2007).
76. S.M. Aouadi, Y. Paudel, B. Luster, S. Stadler, P. Kohli, C. Muratore, C. Hager, A.A. Voevodin, *Tribol. Lett.* **29**, 95 (2008).
77. B.C. Stupp, *Thin Solid Films* **84**, 257 (1981).
78. P. Neiderhäuser, H.E. Hintermann, M. Maillat, *Thin Solid Films* **108**, 209 (1983).
79. T. Spalvins, *Thin Solid Films* **118**, 375 (1984).
80. L.E. Pope, T.R. Jarvis, M. Nastasi, *Surf. Coat. Technol.* **42**, 217 (1990).
81. J.S. Zabinski, M.S. Donley, V.J. Dyhouse, N.T. McDevitt, *Thin Solid Films* **214**, 156 (1992).
82. K.J. Wahl, I.L. Singer, *Tribol. Lett.* **1**, 59 (1995). □



For Variable Temperature Micro Probes I depend on MMR.

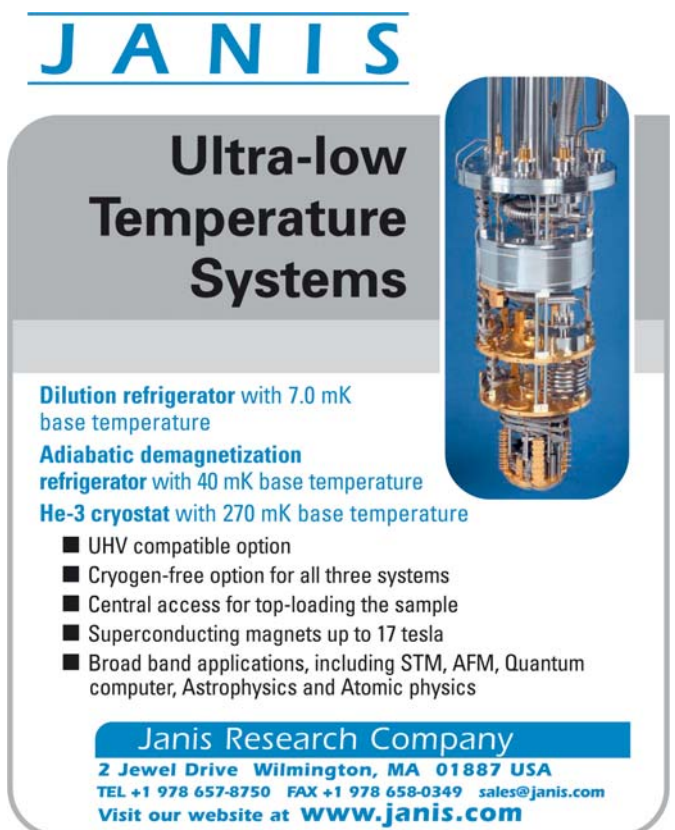
Programmable temperature cycling from 70K to 730K. Without LN₂! And you can choose from 1 to 7 high-precision probes.

Sample-change is quick. And viewing is easy through a clear, frost-free window. These compact systems are ideal for DLTS, materials studies, testing ICs and IR detectors and more...

Best of all, they're from MMR!

To learn more... call (650) 962-9620 or go to the MMR website:

www.mmr.com



JANIS

Ultra-low Temperature Systems

Dilution refrigerator with 7.0 mK base temperature

Adiabatic demagnetization refrigerator with 40 mK base temperature

He-3 cryostat with 270 mK base temperature

- UHV compatible option
- Cryogen-free option for all three systems
- Central access for top-loading the sample
- Superconducting magnets up to 17 tesla
- Broad band applications, including STM, AFM, Quantum computer, Astrophysics and Atomic physics

Janis Research Company
 2 Jewel Drive Wilmington, MA 01887 USA
 TEL +1 978 657-8750 FAX +1 978 658-0349 sales@janis.com
 Visit our website at **www.janis.com**